Transport Models of Ammonium Nitrogen in Wastewater from Rare Earth Smelteries by Reverse Osmosis Membranes

Shuanglin Gui [1,2], Zhaohuan Mai [2,*], Jiaqi Fu [2], Yuansong Wei [2,3] **and Jinbao Wan [1,*]**

1   College of Environmental Resources and Chemical Engineering, Nanchang University, Nanchang 330029, China; gsl503@163.com
2   Institute of Energy Conversion, Jiangxi Academy of Sciences, Nanchang 330096, China; fujqcc@163.com (J.F.); yswei@rcees.ac.cn (Y.W.)
3   State Key Joint Laboratory of Environmental Simulation and Pollution Control, Research Center for Eco-Environmental Sciences, Chinese Academy of Sciences, Beijing 100085, China
*   Correspondence: vivianmzh@hotmail.com (Z.M.); jinbwan@163.com (J.W.)

Abstract: Wastewater from rare earth smelteries contains large amounts of ammonium nitrogen (NH_4^+-N), which causes severe environmental problems. In this contribution, the desalination efficiency of reverse osmosis (RO) was investigated in the treatment of NH_4Cl or $NaCl$ solutions from 0.1 to 40 g/L under different operating pressures with a commercial RO membrane. Experimental results showed that when an operating pressure above 30 bar is applied to the 5 g/L NH_4Cl solution, the permeate was found to meet the discharge standards of NH_4^+-N. Compared to NH_4Cl, the permeate fluxes of $NaCl$ solutions were higher due to the higher net driving force and lower propensity to membrane fouling. Theoretical models indicate a linear relationship between water flux and the net driving force for both NH_4Cl and $NaCl$ solutions. On the contrary, a power function between the salt flux and concentration difference correlated well with the experimental data for salt transport. The equations for water and salt transport obtained by this work would provide a facile and practical means for predicting the membrane performance in design and optimization of RO processes for the treatment of wastewater from the rare earth industry.

Keywords: ammonium nitrogen; reverse osmosis; mass-transfer model; concentration polarization; rare earth industry

1. Introduction

In the past two decades, the demand for rare earth elements (REEs) underwent an explosion due to the widespread application of REEs in daily life, such as cell phones, computer memory, rechargeable batteries, fluorescent lighting, magnets, etc [1]. China has abundant rare earth resources, which contribute an average share of over 85% to the global REEs supply in the last twenty years [2]. However, during the REEs smelting process, large quantities of chemicals are used. Especially in the extraction stage, ammonium hydroxide (NH_4OH) is added to saponify the acidic extractants, resulting in an annual discharge of ten million tons of wastewater with a high content of ammonium nitrogen (NH_4^+-N), which generally ranges from 300 to 40,000 mg/L in different stages (e.g., extraction, precipitation and washing stages) and is far above the national discharge standards in the rare earth industry (GB26451-2011) [3–5]. Furthermore, it is reported that the washing wastewater from the REEs precipitation process mainly contains NH_4^+-N, while other parameters (e.g., REEs, heavy metals, COD, TP) are lower than the discharge standards [6,7]. Direct discharge of wastewater with high content of NH_4^+-N will not only waste a lot of resources, but will also induce high environmental risks, such as

eutrophication and excessive propagation of algae [3]. Therefore, developing reliable technologies for NH_4^+-N discharge in the rare earth industry is of great concern for sustainable water reuse and cleaner production from the economic and environmental perspectives.

Conventional technologies, such as ammonia stripping, evaporation crystallization and struvite precipitation, are widely applied in high strength NH_4^+-N wastewaters [6–8]. However, the disadvantages of these methods such as high energy consumption, secondary pollution and/or demand for advanced treatment to meet the discharge standards, render them techno-economically inefficient and hinder their wider applications. Biochemical technologies also present significant challenges in high strength NH_4^+-N wastewaters because of the high salt concentration and lack of organics [6,7].

Membrane technology, especially reverse osmosis (RO), featured as environmentally friendly, easy to operate and requiring no additional chemicals, stands out as a competitive alternative to treat rare earth wastewater [9]. The driving force of RO is pressure difference, that is, when the operating pressure is higher than the osmotic pressure of the feed solution, water molecules can pass through the RO membrane, and most of the raw water in the inorganic salts, organic matter, colloid and microorganisms will be retained for the size sieve effect of the RO membrane. RO is mostly used for the desalination of brackish water with salt concentration under 10,000 mg/L and seawater with salt concentration in the range of 35,000–40,000 mg/L for their high efficiency on the separation/concentration of organic matters, salts and even monovalent ions [10]. The reported values of NH_4^+-N concentration in wastewater generated from the rare earth industry fall in the range of salt concentrations in brackish water and seawater RO membranes. Thus, RO is expected to have potential as an advanced wastewater treatment technology for rare earth smeltery wastewater with high concentrations of NH_4^+-N.

However, the application of RO in treating rare earth smeltery wastewater is rather limited, and the literature of RO application in the rare earth industry is scarce. Zhang et al. proposed an air stripping and low-pressure reverse osmosis (LPRO) combined process for the treatment of rare earth smeltery wastewater containing high concentrations of NH_4^+-N [11]. The LPRO desalination process showed high retention efficiencies of ammonia with a rejection of 95% as the NH_4^+-N concentration of the feed solution was 200–300 mg/L, and the permeate could be directly discharged or reused. Huang et al. studied the feasibility of RO for rare earth ammonium nitrogen wastewater, and proved that the RO membrane could be used as pre-treatment when the NH_4Cl concentration of real wastewater was 2.85 g/L [12]. Moreover, many researchers focused on the application of RO processes in the removal of NH_4^+-N in other effluents [13–15]. Chang and Chung used spiral wound RO for ammonium pre-concentration prior to ion exchange [12].The rejection of the RO membrane in their study was only 10% and the permeate concentration of NH_4^+-N was 8450 mg/L. Bódalo et al. investigated the performance of a cellulose acetate RO membrane in a cross-flow module for the treatment of aqueous solutions containing 55–9545 mg/L NH_4^+-N [13]. A solution–diffusion model was applied to understand the mass transfer through the RO membrane, and a high rejection of NH_4^+-N (>98.6%) was observed. These results proved the feasibility of RO to decrease the concentration of NH_4^+-N in feed solutions. However, there are only a few studies on testing raw effluents with high concentration of NH_4^+-N. In addition, the current research on rare earth wastewater mainly focuses on the treatment technology and process while the investigation of the mass-transfer process of rare earth wastewater in an RO membrane is rather limited. Therefore, a systematic study to examine the efficiency of RO for the desalination of high NH_4^+-N wastewater and water/salt mass transfer behavior through RO membranes is desirable.

As a permselective barrier, RO membrane performance is mainly determined by water flux and solute rejection [16]. Both parameters are dependent on membrane properties, wastewater composition, and environmental and operating conditions. Therefore, predictive modelling of water flux and salt rejection in aqueous solutions by RO membranes is important for the optimization and scale-up of the water treatment processes. Many researchers have investigated the mass transfer of salts by modeling the RO process [17–23]. The most commonly accepted model of RO was developed by Merten and

Lonsdale based on the solution–diffusion mechanism [17,18]. This model considered that both water and solute transport through a dissolution–diffusion–desorption process. Water is driven by pressure differences across the membrane in RO, whereas the transport of salts or ions is driven by a concentration gradient in the feed and the permeate. With this model, a linear relation is commonly expected between water flux and the pressure difference. But the nonlinear relationship of water flux has been observed under high salt concentrations in several lab-scale experiments, which could be explained by an alternative expression of the driving force [24]. On the other hand, according to Merten and Lonsdale's model, the salt flux is considered linearly related to the concentration differences. However, a power function relationship has also been reported [24]. It has been widely noted that classical transport theories and models become inconvenient to describe complex separation and transport phenomena. Hence, it is necessary to establish simple but practical transport equations to interpret experimental observations, and thus offer a clear guideline on improving the membrane performance.

The main objective of this study was thus to explore the applicability of RO for the treatment of the wastewater with highly concentrated NH_4^+-N from a rare earth smeltery and investigate the mass transfer mechanism. Simulated NH_4Cl and $NaCl$ solutions in different concentrations were tested under different operating pressures in a lab-scale setup. Theoretical and practical equations for water and salt fluxes through RO membranes were proposed based on classical theories and the observed experimental data, to investigate the water and salt transport, and to predict the RO membrane performance in real rare earth wastewater treatment. This contribution offers a new approach to the treatment and reuse of the high NH_4^+-N wastewater by RO.

2. Theory

According to the solution–diffusion model established by Merten and Lonsdale [17,18], the water flux in the RO process can be expressed as a linear function of the net driving force, which can be calculated by the following equation:

$$J_v = A(\Delta p - \Delta \pi) \tag{1}$$

where J_v is water flux (L/m^2 h), A is the water permeability constant or water transport coefficient of the membrane (L/m^2 h bar), $(\Delta p - \Delta \pi)$ is the net driving force in which Δp and $\Delta \pi$ represent the hydraulic pressure difference (bar) and osmotic pressure difference across the membrane (bar), respectively.

The water transport coefficient A is a constant for a given membrane and salt concentration, it was calculated as follows [22]:

$$A = \frac{D_w N_w V_w}{RTL} \tag{2}$$

where D_w and N_w are the diffusion coefficient and solubility of water inside the membrane, respectively, V_w is the molar volume of water, R is the gas constant, T is the temperature and L is the thickness of the membrane functional layer.

The osmotic pressure $\Delta \pi$ in Equation (1) is calculated as follows:

$$\Delta \pi = iRT\Delta C_s = iRT\left(C_{f,s} - C_{p,s}\right) \tag{3}$$

where i is the number of dissociated ions from the dissolved salt s, ΔC_s is the salt concentration difference (g/L) between the feed and the permeate, and $C_{f,s}$ and $C_{p,s}$ are concentrations of salt s in the feed and permeate solution, respectively.

The apparent salt rejection to component s, $R_{app,s}$, was determined using the following equation:

$$R_{app,s} = 1 - \frac{C_{p,s}}{C_{f,s}} \tag{4}$$

Combining Equations (3) and (4) yields:

$$\Delta \pi = iRTR_{app,s}C_{f,s} = R_{app,s}\pi_{f,s} \tag{5}$$

where $\pi_{f,s}$ is the feed osmotic pressure (bar).

The following equation is derived from Equation (1):

$$J_v = A\left(\Delta p - R_{app,s}\pi_{f,s}\right) \tag{6}$$

From the classical salt transport theory, the salt flux J_s (mol/m^2 h) can be expressed as a linear function of the concentration difference between the feed and the permeate, using the solution–diffusion model [17–22]:

$$J_s = -D_s\frac{dC_s}{dx} = \frac{D_sK_s}{L}\left(C_{f,s} - C_{p,s}\right) = B\left(C_{f,s} - C_{p,s}\right) = BR_{app,s}C_{f,s} \tag{7}$$

where D_s and K_s are the salt diffusion coefficient inside the membrane and salt sorption coefficient between the membrane and the feed solution, respectively, and B is the salt permeability constant or salt transport coefficient (L/m^2 h).

The permeate salt concentration, $C_{p,s}$, is determined by:

$$C_{p,s} = \frac{J_s}{J_v} \tag{8}$$

With Equations (4), (7) and (8), the salt rejection can be derived to the following expression:

$$\frac{1}{R_{app,s}} = B\frac{1}{J_v} + 1 \tag{9}$$

From the above equations, it can be assumed that if the linear relationship as stated in Equation (7) was correct and the plot of $1/R_{app,s}$ vs. $1/J_v$ should be a straight line with the same slope B.

3. Materials and Methods

3.1. Wastewater Characteristics

According to the characteristics of the wastewater from a rare earth separation plant in south China, the concentration of NH_4^+-N in wastewater from the extraction stage was as high as 39 g/L, while that of wastewater from the precipitation and washing stage was 0.9–10 g/L [6,7]. It should be noted that an excess of HCl is commonly used to dissolve REEs in the ore. In addition, NaOH is always added instead of NH_4OH for the saponification during the extraction stage. As a result, the wastewater contains a considerable amount of Na$^+$ and Cl$^-$ as NH_4^+-N, but due to its non-toxic properties, the concentration of Na$^+$ has rarely been reported in the rare earth wastewater. Consequently, to be more realistic, both ammonium chloride (NH_4Cl) and sodium chloride (NaCl) were chosen as model solutes for the RO tests in this study.

In addition, wastewater samples of the washing stage were collected from a rare earth plant in Nanchang (Jiangxi, China) to validate the accuracy of the transport models established from RO membrane performance parameters with synthetic solutions. The compositions of the real wastewater and synthetic wastewater are summarized in Table 1.

Table 1. Concentration of main pollutants in the real wastewater and the synthetic wastewater.

Concentration (mg/L)	pH	NH_4^+-N	COD	As^{3+}	Pb$^{2+/4+}$	Cl$^-$
Real wastewater	6.4 ± 0.1	$1.14 \times 10^3 \pm 39$	46 ± 1.8	0.27 ± 0.008	0.15 ± 0.006	$2.95 \times 10^3 \pm 58$
Synthetic wastewater	6.5 ± 0.1	$(0.1\text{–}40) \times 10^3$	/	/	/	$(0.1\text{–}40) \times 10^3$
Indirect discharge standards	6–9	50	100	0.1	0.2	/

3.2. Materials

Commercial flat-sheet SG membranes (GE Osmonics, Minnetonka, MN, USA) with smooth surface, fouling-resistant and high retention rate against sodium chloride were used in this study,

which has an effective separation area of 0.014 m^2. The detailed information on the structure, properties, and operating parameters of the SG membrane was described elsewhere [25,26]. All membranes were equilibrated with distilled water for at least 24 h and stored in 5 °C prior to use.

Ammonium chloride (NH$_4$Cl, reagent grade, Xilong Scientific, Shantou, China) and sodium chloride (NaCl, reagent grade, Xilong Scientific, Shantou, China) were used to make synthetic wastewater of REEs. Salt solutions were prepared with deionized water (DI water, resistance > 18 MΩ) throughout this study.

3.3. Experimental Setup

A lab-scale cross-flow RO setup equipped with a stainless steel membrane module unit (SEPA CF II, GE Osmonics, Minnetonka, MN, USA) was used to investigate the membrane and variations of transport properties [27]. The RO system is exhibited in Figure 1; the system consists of a 30 L stainless steel feed tank, a high-pressure diaphragm pump (Hydro-Cell M-03S, Wanner Engineering, Minneapolis, MN, USA) controlled by a frequency converter, a feed flow meter, two pressure gauges, two bypass valves, and other accessories. A piece of flat sheet SG membrane was fixed in the cell with a feed spacer and shims. The batch experiment was conducted in a closed-loop mode, that is the feed stream was pumped from the feed tank to the membrane unit and the retentate and permeate were re-circulated back to the feed tank to keep the concentration of feed solution constant. The feedwater temperature was maintained constant by a recirculating heater/chiller (PolyScience, Niles, IL, USA). Adjustment of the transmembrane pressure and the cross-flow velocity was achieved through the pressure gauges and bypass valves located in the inlet and outlet of the membrane cell.
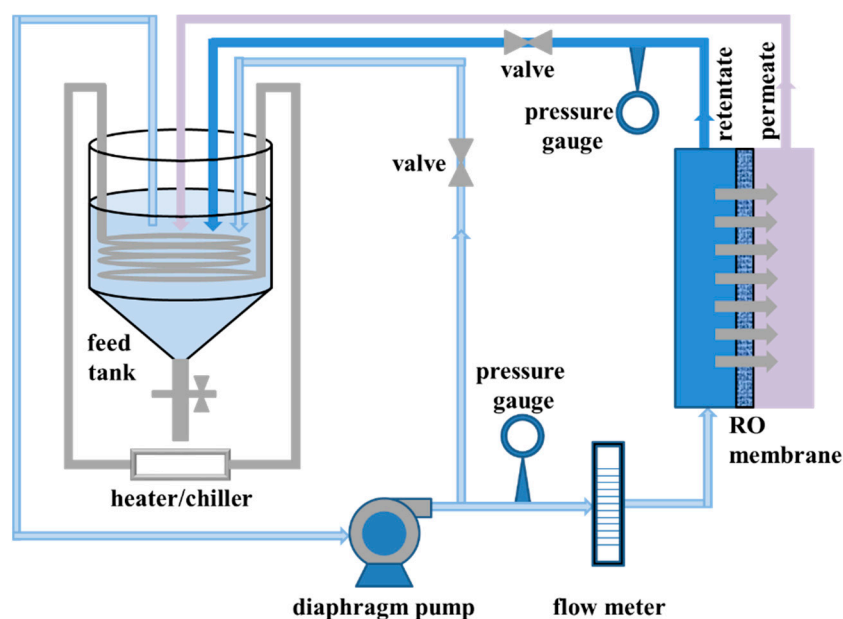
Figure 1. Schematic diagram of the lab-scale reverse osmosis (RO) setup.

3.4. Experimental RO Process

3.4.1. Synthetic Salt Solutions

Synthetic salt solutions were used in the study of RO membrane performance. For NH$_4$Cl solutions, concentrations of 0.1, 0.5, 1, 5, 10, 20, and 40 g/L were selected, respectively. The concentrations of NaCl solutions were set as 0.5, 1, 5, 10, 20, and 40 g/L, respectively.

Prior to each set of filtrations, SG membranes were pre-cleaned following the procedures recommended by the manufacturer: the membrane was firstly rinsed with distilled water for 20 min, followed by a caustic wash with an NaOH solution (pH = 10–10.5) for 30 min, and finally rinsed with

distilled water again until the pH returned to neutral. All the pre-cleaning procedures were conducted at 45 °C and at an operating pressure of 30 bar.

The test membranes were then compacted with DI water at 30 bar for at least 2 h until a steady constant permeate flux was obtained and pure water flux was measured. Subsequently, salt solutions with different compositions were fed to the RO set-up under a flow rate of 0.5 m/s. The filtration experiments of each salt solution were performed at 25 °C under multiple operating pressures ranging from 15 to 40 bar (unless otherwise specified in some high concentration cases) with a pressure interval of 5 bar. The salt concentrations of the permeate and the feed were measured by a DDSJ-308A conductivity meter (Leici Company, Shanghai, China) after 4 h of continuous operation to achieve a stable performance. In some low concentration cases, the salt concentrations of NH_4^+ in the permeate were measured by Kjeldahl determination, and the concentration of Na^+ in the permeate was measured by an inductively coupled plasma atomic emission spectrometry Agilent 5110 ICP-OES (Agilent Technologies, Palo Alto, CA, USA). Steady state water flux under each feed salt concentration or operating pressure was also recorded.

3.4.2. Real Wastewater Treatment

The raw washing wastewater obtained from the rare earth plant was tested with an SG membrane under 30 bar. The other operating conditions were the same as in the previous part.

3.4.3. Determination of Water and Salt Permeabilities

For both synthetic and real wastewater, the steady-state permeate flux, J_v (L/h·m^2) was calculated as follows:

$$J_v = \frac{V}{t \times A_m} \tag{10}$$

where V is the volume of the collected permeate (L), t is the sampling duration (h), and A_m is the effective membrane area (m^2).

The apparent salt rejection was calculated according to Equation (4). Permeate flux and solute concentration were measured for at least two consecutive samples (obtained at a given set of experimental conditions), with the average deviation below 3%. For each case of given feed salt concentration and operating pressure, at least two sets of experiments were conducted to gauge the variability between different membranes. The average values of the comparative experiments were presented, accompanied with the standard deviations.

4. Results and Discussion

4.1. NH$_4$Cl Removal Performance of RO Membrane

The dependence of (a) permeate flux J_v and (b) apparent rejection $R_{app,NH4Cl}$ on operating pressure at different NH$_4$Cl concentrations are plotted in Figure 2. It can be found that the water flux increases with the operating pressure for a given salt concentration. For 1 g/L NH$_4$Cl solution, the flux gradually increases from 17.86 L/m^2 h at 15 bar to 40.48 L/m^2 h at 35 bar. It can be explained by Equation (1) that at the same salt concentration, the increase of operating pressure would enhance the net driving force for water transport, thus resulting in a higher water flux. Especially, the relationship between pure water flux and the operating pressure was found to be linear, and plotting J_v vs. Δp in Figure 2a yields the value of A in Equation (1) equal to 1.96 L/m^2 h bar. The determined pure water permeability of the SG membrane just falls in the A-value ranges of commercially available polyamide seawater membranes [28], but is slightly lower than the values reported in previous studies for the SG membrane (2.46 L/m^2 h bar), possibly due to different filtration configurations and operating conditions [25,26].
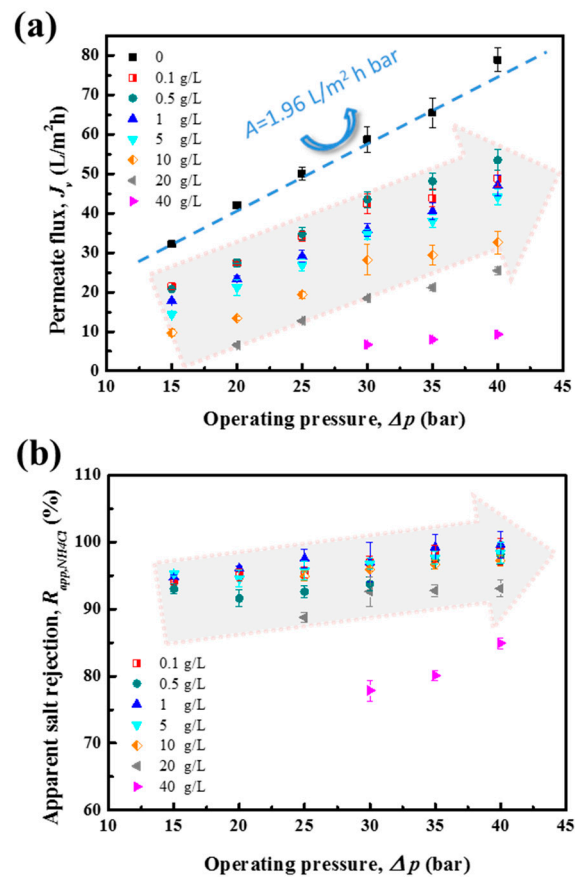
Figure 2. (**a**) Permeate flux J_v and (**b**) apparent rejection $R_{app,NH4Cl}$ vs. operating pressure Δp at different feed concentrations of NH$_4$Cl solution for the SG membrane.

As shown in Figure 2a, there is also a strong correlation between water flux and the NH$_4$Cl concentration in the feed solution. The water flux decreases with increasing NH$_4$Cl concentration. An elevated concentration yields a higher osmotic pressure and thus reduces the net driving force, as described in Equations (3) and (1), respectively. It is interesting that there was almost no permeate flux of the 20 g/L feed solution at operating pressures below 20 bar, mainly because at this condition, the calculated osmotic pressure (Equation (5)) in the upstream of the membrane was as high as 18.53 bar. The net driving force ($\Delta p - \Delta \pi$) presented only a weakened drive of water molecules across the SG membrane. However, at 40 g/L, a very low permeate flux was still observed at 30 bar even though $\pi_{f,s}$ was 37.06 bar at this concentration. This might be caused by the low rejection of NH$_4$Cl ($R_{app,NH4Cl}$ = 77.87%) which contributed to $\Delta \pi$ = 28.86 bar in this case. Furthermore, the increase of salt concentration was reported to enhance the viscosity of the salt solution, which might lead to a slower diffusion process of the water molecules in the membrane, thereby causing a decline of the water flux [29].

The effect of operating pressure and salt concentration on the apparent NH$_4$Cl rejection is exhibited in Figure 2b. The general trend for all feed solutions indicates that the apparent salt rejection increases with the operating pressure, which is consistent with previous observations for RO and NF [14,29]. When the concentrations below 10 g/L, the rejection of NH$_4$Cl slightly decreases with the increase of NH$_4$Cl concentration in the feed water. In contrast, at higher concentrations, $R_{app,NH4Cl}$ drops dramatically to around or even below 90%. According to Equation (8), the permeate salt concentration, $C_{p,\,NH4Cl}$, is dependent on the ratio of salt flux to water flux. The salt flux, J_s, as indicated in Equation (7), is driven by the concentration difference and is approximately independent of pressure. Generally speaking, increasing the salt concentration in feeds enlarges the salt concentration difference between the feed and the permeate. Therefore, the driving force for salt transport is enhanced

accordingly, leading to an enhanced NH$_4$Cl permeation. Thus, the apparent salt rejection was reduced. Furthermore, as aforementioned, it was inferred that increasing the operating pressure yields a higher water flux, resulting in a lower NH$_4$Cl concentration in the permeate; consequently, the apparent salt rejection was augmented. Moreover, concentration polarization at high feed concentration also decreased the observed rejection.

In concentrated systems (e.g., 20 and 40 g/L NH$_4$Cl), the osmotic pressure is significantly high. Thus, the volumes of the collected permeate were not sufficient for concentration measurement, and as a result, it was difficult to calculate the apparent rejection of these solutions.

From the above discussion, it is noticeable that the removal efficiency of SG membranes is considerable, especially at low NH$_4$Cl concentrations (<10 g/L). The rejection of NH$_4$Cl ranged from 77.87% to 99.58% and the permeate flux was between 6.69 and 53.14 L/m^2 h in the studied range of pressures and feed concentrations. As the NH$_4^+$-N concentration of feed solution was 1.31 g/L (corresponding to 5 g/L NH$_4$Cl), the permeate could meet the emission standards of NH$_4^+$-N in the rare earth industry (50 mg/L for indirect discharge) when operating pressure was above 30 bar. Thus, it can be concluded that wastewater containing 1.31 g/L NH$_4^+$-N or below can be discharged or reused by the RO process with the SG membrane without additional treatment.

4.2. NaCl Removal Performance of RO Membrane

Figure 3 represents the influence of operating pressure and feed concentrations of NaCl on the (a) permeate flux J_v and (b) apparent rejection of $R_{app,NaCl}$, in equilibrium state for SG membranes. The permeate flux and apparent rejection of NaCl increase with operating pressure, while both decreased with the increasing feed concentration. Moreover, the undetected permeate flux and apparent salt rejection at low pressures in 40 g/L solution can also be explained by the high osmotic pressure and the phenomenon of concentration polarization, as discussed in the previous section.
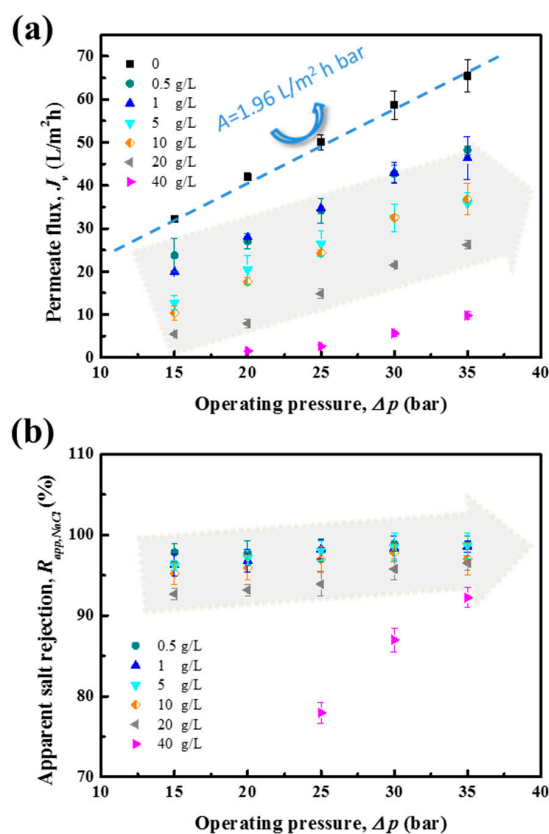
Figure 3. (**a**) Permeate flux J_v and (**b**) apparent rejection of $R_{app,NaCl}$ vs. operating pressure Δp under different feed concentrations of NaCl solution for the SG membrane.

In general, the dependence of permeate flux and apparent salt rejection on operating pressure and feed concentration of NaCl solutions is similar to that of NH$_4$Cl solutions. However, there are some differences in the water and salt transport between the two salt solutions. Firstly, the permeate flux of NaCl solutions in the RO process with an SG membrane was found to be relatively higher under the same experimental conditions at low concentrations (<10 g/L). The reason was believed to be the higher molar concentration of NH$_4$Cl at the same mass concentration of NH$_4$Cl and NaCl, which causes higher osmotic pressure and lower driven force. Secondly, the concentration polarization was more severe for the NH$_4$Cl solution. It was found that the concentration polarization was noticeable especially at lower transmembrane pressures for 20 g/L NH$_4$Cl solution. As a result, a dense crystal layer might be formed on the membrane surface, thus preventing the mass transfer of NH$_4$Cl molecules. Permeate flux was still observed at a relatively low rate, even though the applied operating pressure was only 15 bar as RO was applied in the NaCl solution with the same concentration. Thus, it can be concluded that the NH$_4$Cl solution has a higher fouling propensity to the SG membrane compared to NaCl at high concentrations.

Typical RO membranes are composed of three layers: a top dense and selective polyamide layer, an intermediate microporous polysulfonate layer, and a non-woven fabric support layer. By using positron annihilation spectroscopic technology, Kim et al. determined that the radius of the network pore and the aggregate pore of polyamide layer of the thin film composite (TFC) membrane were about 0.20 and 0.45 nm, respectively [30]. Transport would be strongly hindered when the size of the pore was smaller than the hydrated radius. In this study, the apparent salt rejection of NaCl was observed to be slightly higher than that of NH$_4$Cl under the same operating conditions. The selectivity between Na$^+$ and NH$_4^+$ that was based on the hydration exclusion in the RO membrane was attributed to be the main reason [31–34]. The hydrated ion radius of Na$^+$ (3.58 Å) was larger than that of NH$_4^+$ (3.31 Å) [21,23], which led to make it more difficult for the sodium ions to penetrate the membrane. This was consistent with the hydration energy of the ions, where the value of hydration energy of Na$^+$ (−454 kJ/mol) was higher than that of NH$_4^+$ (−331 kJ/mol) [31,32]; that well explains the higher rejection for NaCl. In other words, the apparent rejection order of the two salt solutions is similar to the order of the hydration energy and hydration ion radius for the monovalent ions.

4.3. Transport Models for Water and Salt Flux

To examine the validity of the water transport model described in Equation (6), the permeate flux is plotted vs its net driving force ($\Delta p - R_{app,s}\pi_{f,s}$) at different concentrations for both NH$_4$Cl and NaCl solutions, as illustrated in Figures 4 and 5, respectively. It is shown that for all concentrations tested in this study, the permeate flux increased linearly with the net driving force. The slopes obtained by linear regression corresponded to the water transport coefficients (*A*) of the salt solutions, as presented in Equation (6). It can be seen from Figure 4 that the permeability coefficient of an NH$_4$Cl solution is 1.29 L/m^2 h bar, which is slightly lower than the permeability coefficient of an NaCl solution (1.35 L/m^2 h bar) obtained from Figure 5. Generally, the higher the *A*-value, the higher the productivity of water. This is coincident with the results in the previous section, where the permeate flux of the NaCl solution was higher than that of the NH$_4$Cl solution at the same concentration. Both *A*-values of the salt solutions were lower than the pure water permeability coefficient and were consistent with the *A*-values of high salinity solutions in RO processes reported in the literature [22,28]. The good agreement between literature data and predicted data from this study proves the efficiency and accuracy of the transport model described in Equation (6) for calculating the water flux during RO. Furthermore, the permeability coefficient *A* is determined by the membrane property, and is independent of operating conditions, such as pressure and salt concentration. Thus, it can be used for RO performance evaluation and prediction in the application of rare earth wastewater desalination with concentrations of NH$_4$Cl or NaCl up to 40 g/L.
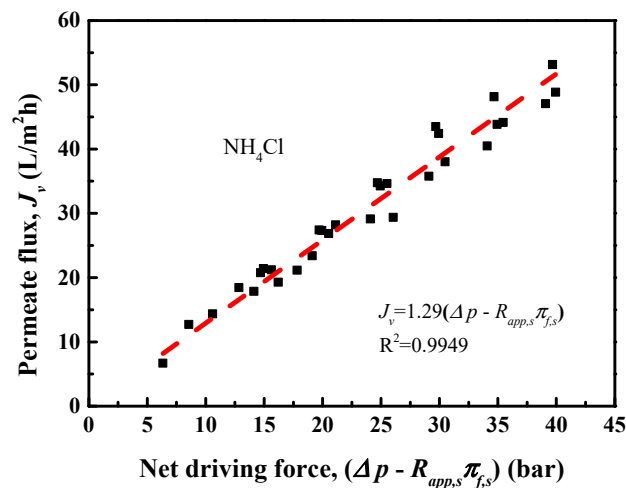
Figure 4. Correlation of permeate flux with the net driving force at different feed concentrations of NH₄Cl solutions. The slope of the curve-fitting is the *A*-value in Equation (1) for SG membranes with NH₄Cl solutions.
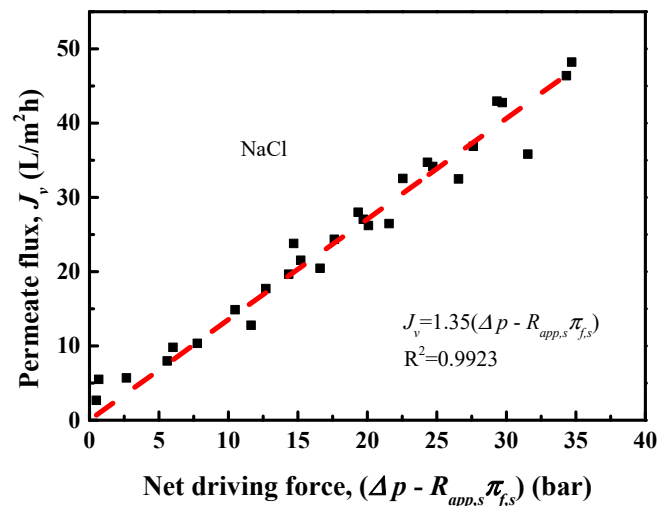
Figure 5. Correlation of permeate flux with the net driving force at different feed concentrations of NaCl solutions. The slope of the curve-fitting is the *A*-value in Equation (1) for SG membranes with NaCl solutions.

As for the salt transport during the RO process, it was assumed that if the salt permeability coefficient *B* in Equation (7) is constant, the linear relationship between $1/R_{app,s}$ and $1/J_v$ in Equation (9) would hold true. However, the experimental rejection data for the SG membrane with both NH₄Cl and NaCl solutions produced curves rather than straight lines as plotted in Figures 6 and 7 for each salt. The *B*-values and R^2 values from regression are listed in Table 2. The low R^2 values indicate that salt fluxes through the SG membrane might not be accurately described with the linear relationship of the corresponding driving force. Since the separation and transport mechanism of membranes are complicated, the effect of a concentration gradient on salt transport is always found to deviate from a linear trend [24].
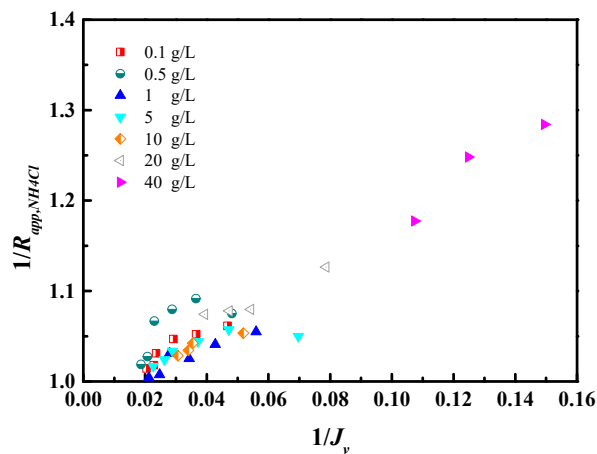
Figure 6. The correlation of $1/R_{app,NH4Cl}$ and $1/J_v$ at different feed concentrations of NH$_4$Cl solutions.
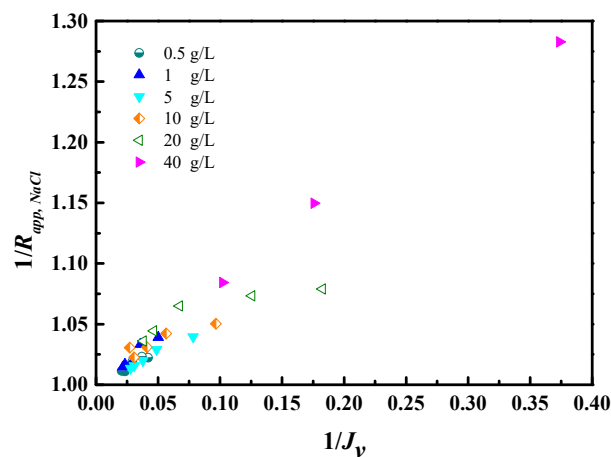
Figure 7. The correlation of $1/R_{app,NaCl}$ and $1/J_v$ at different feed concentrations of NaCl solutions.

Table 2. Summary of the regression coefficient B and R^2 values with Equation (9) for NH$_4$Cl and NaCl solutions.

NH$_4$Cl			NaCl		
C_f (g/L)	B (L/m^{2}h)	R^2 Value	C_f (g/L)	B (L/m^{2}h)	R^2 Value
0.1	1.29	0.7886	0.1	-	-
0.5	2.02	0.4879	0.5	0.57	0.8650
1	0.86	0.7269	1	0.78	0.8855
5	0.93	0.5400	5	0.53	0.9666
10	1.05	0.8776	10	0.63	0.2095
20	1.62	0.9011	20	0.55	0.342
40	1.8707	0.8671	40	0.78	0.9876

　　　Recently, a reformulated solution–diffusion model incorporating activity coefficients was proposed for solute transport in RO/NF [35,36]. In this model, the salt concentration was corrected with salt activity, which has a strong nonlinearity with the actual measured salt concentrations, to calculate the solute transport. Neglecting the salt activity might explain the erratic phenomenological *B*-values observed in the literature and in this work.

　　　Since theoretical models contain several coefficients, it is much more practical to establish simple mathematical equations instead of complicated theoretical models for optimizing operational processes

during the treatment of industrial wastewaters. Herein, a power relationship between salt flux and the concentration difference is assumed in the salt transport. The mathematical equation is hypothesized as follows [24]:

$$J_s = \beta \left(C_{f,s} - C_{p,s} \right)^{\alpha} \tag{11}$$

where β is a correlation coefficient and α is the power function coefficient. With Equations (8) and (11), the following equation is derived:

$$\log \left[J_v C_{f,s} \left(1 - R_{app,s} \right) \right] = \alpha \log \left(C_{f,s} R_{app,s} \right) + \log \beta \tag{12}$$

The parameters α and β can be obtained from the linear regression of $\{\log[J_v C_{f,s} (1 - R_{app,s})]\}$ with $\{\log(C_{f,s} R_{app,s})\}$. The plots of $\{\log[J_v C_{f,s} (1 - R_{app,s})]\}$ vs. $\{\log(C_{f,s} R_{app,s})\}$ at different operating pressures are shown in Figures 8 and 9 for NH$_4$Cl and NaCl solutions, respectively. The coefficients α and β as well as R^2 values for the transport of NH$_4$Cl and NaCl are summarized in Table 3. The high R^2 values indicate that the proposed power function relationship for salt transport fits the experimental data satisfactorily.
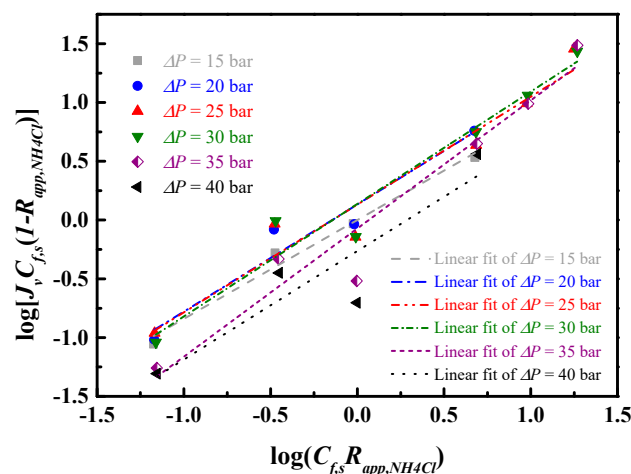
Figure 8. Correlation of $\log[J_v C_{f,s} (1-R_{app,NH4Cl})]$ with $\log(C_{f,s} R_{app,NH4Cl})$ determined with Equation (12), to investigate the possibility of a power relation between salt flux and the concentration difference of NH$_4$Cl solution. The linear fit lines show good linearity.
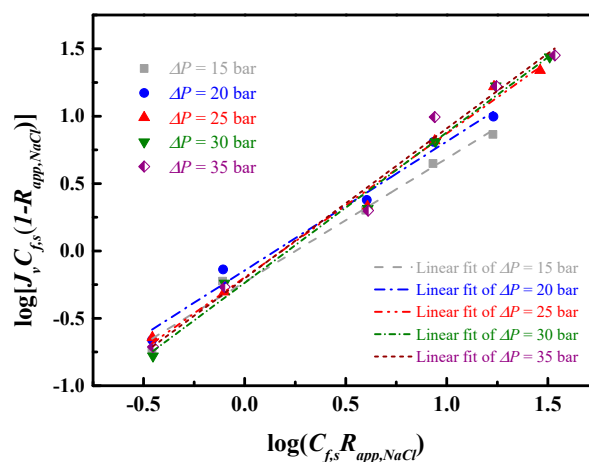
Figure 9. Correlation of $\log[J_v C_{f,s} (1-R_{app,NaCl})]$ with $\log(C_{f,s} R_{app,NaCl})$ determined with Equation (12) to investigate the possibility of a power relation between salt flux and the concentration difference of NaCl solution. The linear fit lines show good linearity.

Table 3. Summary of regression coefficient α, β and R^2 values with Equation (12) for NH_4Cl and NaCl solutions.

Operating Pressure (bar)	NH$_4$Cl			NaCl		
	α	β	R^2 Value	α	β	R^2 Value
15	0.84	1.00	0.9846	0.92	0.59	0.9882
20	0.91	1.36	0.9491	0.96	0.72	0.9862
25	0.92	1.36	0.9494	1.07	0.64	0.9919
30	0.96	1.37	0.9634	1.12	0.58	0.9906
35	1.09	0.85	0.9465	1.11	0.63	0.9840
40	0.92	0.54	0.8458	-	-	-

From Table 3, it can be concluded that the coefficient α of the power function showed an increasing trend with operating pressure for each salt, indicating that the nonlinearity of the salt flux increases with operating pressure. The α value of the NaCl solution is slightly higher than that of NH_4Cl at the same operating pressure. Table 3 also demonstrates that the transport coefficient β remains in the range of 0.85–1.37 and 0.58–0.72 for NH_4Cl and NaCl, respectively. To simplify the dependence of transport coefficients on operating conditions, which is desirable in membrane transport for process design and operational optimization, the data in Figure 8 with different operating pressures of NH_4Cl system were plotted together. It can be roughly estimated that the α and β values were independent of pressure and feed salt concentration for the SG membrane; the values were around 0.97 and 1.08, respectively, for the NH_4Cl solutions. The same simplification method was applied to the NaCl system shown in Figure 9, and it was found that the α and β values are around 1.05 and 0.63; these values are also independent of pressure and feed salt concentration for the SG membrane.

To validate the accuracy of the proposed models for water and salt transport, real wastewater from the washing stage in a rare earth plant in Jiangxi Province (China) was tested by the SEPA CF II system with an SG membrane. The concentration of NH_4^+-N in the wastewater was 1.14 g/L, and the operating pressure was 30 bar. The predicted values as well as the experimental data of the permeate flux and apparent rejection to NH_4^+-N are summarized in Table 4. The predicted permeate flux is slightly higher than the experimental data, due to the simplification of the model by overlooking the effect of other trace elements in the wastewater. A good agreement between predicted values and experimental data shows that the proposed equations of water and salt transport are appropriate for the prediction of the membrane performance when dealing with real wastewater.

Table 4. Comparison of the permeate flux and salt rejection between experimental data and predicted values from models with real wastewater from a rare earth plant in the Jiangxi Province (China).

	Experimental Data	Predicted Value from Models
Permeate flux (L/m^{2}h)	31.67	34.77
Apparent rejection to NH_4^+-N (%)	97.53	97.00

5. Conclusions

Commercial RO membranes were used for the desalination of highly concentrated NH_4Cl and NaCl solutions simulated as saline wastewater from the rare earth industry in this work. The apparent salt rejection rates higher than 95% were obtained in most cases for both salts (except for solutions above 20 g/L), indicating the high removal efficiency of SG membranes, and confirming the feasibility of using RO in the treatment of wastewater from the rare earth industry. Especially, the permeate of 5 g/L NH_4Cl solution could meet the requisite discharge standard of NH_4^+-N. A higher rejection and flux was found for sodium compared to NH_4^+-N; the larger hydrated ion size and hydration energy

were the main reasons. The water flux followed a linear pressure-driven process as discovered by mass-transfer modeling. The water permeability coefficient of the NH_4Cl solution (1.29 L/m^2 h bar) and NaCl solution (1.35 L/m^2 h bar) were determined by linear fitting of water flux vs. net driving force, as $J_v = A(\Delta p - R_{app,s}\pi_{f,s})$. However, the salt transport did not show a linear relationship with concentration difference as proposed in classical solution–diffusion theories. Thus, a power function equation as $J_s = \beta(C_{f,s} - C_{p,s})^\alpha$ was proposed to explain the relationship among the feed concentration, water flux, and apparent salt rejection, aimed at the interpretation of the salt transport. All the predicted transport coefficients agreed well with the experimental data, and the models were also validated by real wastewater from a rare earth smeltery. The fundamental study on the elucidation of mass-transfer performance can provide insights to facilitate the application of RO in the treatment of wastewater from the rare earth industry, and to fill the knowledge gaps of understanding the mass transfer mechanism in the RO process.

Author Contributions: Formal analysis, S.G. and Z.M.; investigation S.G., Z.M. and J.F.; project administration, Z.M. and J.W.; supervision, J.W. and Y.W.; writing—original draft preparation, S.G. and Z.M.; writing review and editing, Z.M. and J.W.; funding acquisition, Z.M. All authors have read and agreed to the published version of the manuscript.

Funding: This work was supported by the National Natural Science Foundation of China (No. 21567009), the JiangXi Association for Science and Technology, and the Key Program of Jiangxi Academy of Sciences (2017-YZD2-14, 2018-YZD2-02).

Acknowledgments: We thank all the authors who contributed to this article.

Conflicts of Interest: The authors declare no conflict of interest.

References

1. Hatje, V.; Bruland, K.W.; Flegal, A.R. Increases in Anthropogenic Gadolinium Anomalies and Rare Earth Element Concentrations in San Francisco Bay over a 20 Year Record. *Environ. Sci. Technol.* **2016**, *50*, 4159–4168. [CrossRef] [PubMed]

2. Chen, J.Y.; Zhu, X.H.; Liu, G.; Chen, W.Q.; Yang, D.H. China's rare earth dominance: The myths and the truths from an industrial ecology perspective. *Resour. Conserv. Recycl.* **2018**, *132*, 139–140. [CrossRef]

3. Wang, L.S.; Huang, X.W.; Yu, Y.; Xiao, Y.F.; Long, Z.Q.; Cui, D.L. Eliminating ammonia emissions during rare earth separation through control of equilibrium acidity in a HEH(EHP)-Cl system. *Green Chem.* **2013**, *15*, 1889–1894. [CrossRef]

4. Yin, S.H.; Chen, K.H.; Srinivasakannan, C.; Guo, S.H.; Li, S.W.; Peng, J.H.; Zhang, L.B. Enhancing recovery of ammonia from rare earth wastewater by air stripping combination of microwave heating and high gravity technology. *Chem. Eng. J.* **2018**, *337*, 515–521. [CrossRef]

5. China Ministry of Environmental Protection, Emission Standards of Pollutants from Rare Earths Industry GB 26451-2011 (in Chinese), Beijing, China. Available online: http://www.mee.gov.cn/ywgz/fgbz/bz/bzwb/shjbh/swrwpfbz/201102/t20110210_200521.shtml (accessed on 1 October 2011).

6. Huang, H.M.; Xiao, X.M.; Yan, B. Complex treatment of the ammonium nitrogen wastewater from rare-earth separation plant. *Desalin. Water Treat.* **2009**, *8*, 109–117. [CrossRef]

7. Huang, H.M.; Xiao, X.M.; Yang, L.P.; Yan, B. Removal of ammonia nitrogen from washing wastewater resulting from the process of rare-earth elements precipitation by the formation of struvite. *Desalin. Water Treat.* **2010**, *24*, 85–92. [CrossRef]

8. Li, Y.; Shi, S.Y.; Cao, H.B.; Wu, X.M.; Zhao, Z.J.; Wang, L.Y. Bipolar membrane electrodialysis for generation of hydrochloric acid and ammonia from simulated ammonium chloride wastewater. *Water Res.* **2016**, *89*, 201–209. [CrossRef]

9. Malaeb, L.; Ayoub, G.M. Reverse osmosis technology for water treatment: State of the art review. *Desalination* **2011**, *267*, 1–8. [CrossRef]

10. Pontié, M.; Charcosset, C. Seawater. Brackish Waters, and Natural Waters Treatment with Hybrid Membrane Processes. In *Integrated Membrane Systems and Processes*, 7th ed.; Basile, A., Charcosset, C., Eds.; John Wiley & Sons Ltd.: Hoboken, NJ, USA, 2016; pp. 165–192. [CrossRef]

11. Zhang, L.N.; Xu, B.H.; Gong, J.D.; Bu, T.D. Membrane combination technic on treatment and reuse of high ammonia and salts wastewater in rare earth manufacture process. *J. Rare Earths* **2010**, *28*, 501–503. [CrossRef]

12. Huang, H.M.; Fu, Z.; Xiao, X.M.; Yan, B. Study on treatment of rare-earth ammonium nitrogen wastewater by reverse osmosis(in Chinese). *Chin. J. Environ. Eng.* **2009**, *3*, 1443–1446.

13. Chang, I.S.; Chung, C.M. Pollution prevention for manufacturing of ammonium chloride-an experimental study of wastewater recycling. *Desalination* **2000**, *127*, 145–153. [CrossRef]

14. Bódalo, A.; Gómez, J.L.; Gómez, E.; León, G.; Tejera, M. Ammonium removal from aqueous solutions by reverse osmosis using cellulose acetate membranes. *Desalination* **2005**, *184*, 149–155. [CrossRef]

15. Häyrynen, K.; Pongrácz, E.; Väisänen, V.; Pap, N.; Mänttäri, M.; Langwaldt, J.; Keiski, R.L. Concentration of ammonium and nitrate from mine water by reverse osmosis and nanofiltration. *Desalination* **2009**, *240*, 280–289. [CrossRef]

16. Park, H.B.; Kamcev, J.; Robeson, L.M.; Elimelech, M.; Freeman, B.D. Maximizing the right stuff: The trade-off between membrane permeability and selectivity. *Science* **2017**, *356*, eaab0530. [CrossRef] [PubMed]

17. Merten, U. Flow Relationships in Reverse Osmosis. *Ind. Eng. Chem. Fundam.* **1963**, *2*, 229–232. [CrossRef]

18. Lonsdale, H.K.; Merten, U.; Riley, R.L. Transport properties of cellulose acetate osmotic membranes. *J. Appl. Polym. Sci.* **1965**, *9*, 1341–1362. [CrossRef]

19. Wijmans, J.G.; Baker, R.W. The solution-diffusion model: A review. *J. Membr. Sci.* **1995**, *107*, 1–21. [CrossRef]

20. Paul, D.R. Reformulation of the solution-diffusion theory of reverse osmosis. *J. Membr. Sci.* **2004**, *241*, 371–386. [CrossRef]

21. Geise, G.M.; Paul, D.R.; Freeman, B.D. Fundamental water and salt transport properties of polymeric materials. *Prog. Polym. Sci.* **2014**, *39*, 1–42. [CrossRef]

22. Hung, L.Y.; Lue, S.J.; You, J.H. Mass-transfer modeling of reverse-osmosis performance on 0.5–2% salty water. *Desalination* **2011**, *265*, 67–73. [CrossRef]

23. Zaidi, S.M.J.; Fadhillah, F.; Khan, Z.; Ismail, A.F. Salt and water transport in reverse osmosis thin film composite seawater desalination membranes. *Desalination* **2015**, *368*, 202–213. [CrossRef]

24. Zhou, W.; Somh, L. Experimental study of water and salt fluxes through reverse osmosis membranes. *Environ. Sci. Technol.* **2005**, *39*, 3382–3387. [CrossRef] [PubMed]

25. Akin, O.; Temelli, F. Probing the hydrophobicity of commercial reverse osmosis membranes produced by interfacial polymerization using contact angle, XPS, FTIR, FE-SEM and AFM. *Desalination* **2011**, *278*, 387–396. [CrossRef]

26. Mai, Z.H.; Butin, V.; Rakib, M.; Zhu, H.C.; Rabiller-Baudry, M.; Couallier, E. Influence of bulk concentration on the organization of molecules at a membrane surface and flux decline during reverse osmosis of an anionic surfactant. *J. Membr. Sci.* **2016**, *499*, 257–268. [CrossRef]

27. Mai, Z.H.; Gui, S.L.; Fu, J.Q.; Jiang, C.; Ortega, E.; Zhao, Y.; Tu, W.Q.; Mickols, W.; Bruggen, B.V. Activity-derived model for water and salt transport in reverse osmosis membranes: A combination of film theory and electrolyte theory. *Desalination* **2019**, *469*, 114094. [CrossRef]

28. Stevens, D.M.; Shu, J.Y.; Reichert, M.; Roy, A. Next-Generation Nanoporous Materials: Progress and Prospects for Reverse Osmosis and Nanofiltration. *Ind. Eng. Chem. Res.* **2017**, *56*, 10526–10551. [CrossRef]

29. Yan, Z.Q.; Zeng, L.M.; Li, Q.; Liu, T.Y.; Matsuyama, H.; Wang, X.L. Selective separation of chloride and sulfate by nanofiltration for high saline wastewater recycling. *Sep. Purif. Technol.* **2016**, *166*, 135–141. [CrossRef]

30. Kim, S.H.; Kwak, S.Y.; Suzuki, T. Positron annihilation spectroscopic evidence to demonstrate the flux-enhancement mechanism in morphology-controlled thin-film-composite (TFC) membrane. *Environ. Sci. Technol.* **2005**, *39*, 1764–1770. [CrossRef]

31. Somrani, A.; Hamzaoui, A.H.; Pontie, M. Study on lithium separation from salt lake brines by nanofiltration (NF) and low pressure reverse osmosis (LPRO). *Desalination* **2013**, *317*, 184–192. [CrossRef]

32. Houriez, C.; Real, F.; Vallet, V.; Mautner, M.; Masella, M. Ion hydration free energies and water surface potential in water nano drops: The cluster pair approximation and the proton hydration Gibbs free energy in solution. *J. Chem. Phys.* **2019**, *151*, 174504. [CrossRef]

33. Mohamedou, E.O.; Suarez, D.B.P.; Vince, F.; Jaouen, P.; Pontie, M. New lives for old reverse osmosis (RO) membranes. *Desalination* **2010**, *253*, 62–70. [CrossRef]

34. Pontie, M.; Diawara, C.K.; Rumeau, M. Streaming effect of single electrolyte mass transfer in nanofiltration: Potential application for the selective defluorination of brackish drinking waters. *Desalination* **2002**, *151*, 267–274. [CrossRef]

35. Mickols, W. Substantial Changes in the Transport Model of Reverse Osmosis and Nanofiltration by Incorporating Accurate Activity Data of Electrolytes. *Ind. Eng. Chem. Res.* **2016**, *55*, 11139–11149. [CrossRef]

36. Jang, E.S.; Mickols, W.; Sujanani, R.; Helenic, A.; Dilenschneider, T.J.; Kamcev, J.; Paul, D.R.; Freeman, B.D. Influence of Concentration Polarization and Thermodynamic Non-ideality on Salt Transport in Reverse Osmosis Membranes. *J. Membr. Sci.* **2019**, *572*, 668–675. [CrossRef]